Two-particle spatial correlations in superfluid nuclei

N. Pillet,[1,*] N. Sandulescu,[2] P. Schuck,[3,4,5] and J.-F. Berger[1]
[1]*CEA/DAM/DIF, F-91297 Arpajon, France*
[2]*Institute of Physics and Nuclear Engineering, R-76900 Bucharest, Romania*
[3]*Institut de Physique Nucléaire, CNRS, UMR8608, F-91406 Orsay, France*
[4]*Université Paris-Sud, Orsay, F-91505, France*
[5]*Laboratoire de Physique et Modélisation des Milieux Condensés, CNRS and Université Joseph Fourier, Maison des Magistères, Boîte Postale 166, F-38042 Grenoble Cedex, France*
(Received 1 October 2009; revised manuscript received 13 January 2010; published 19 March 2010)

We discuss the effect of pairing on two-neutron space correlations in deformed nuclei. The spatial correlations are described by the pairing tensor in coordinate space calculated in the HFB approach. Calculations are done using the D1S Gogny force. We show that the pairing tensor has a rather small extension in the relative coordinate, a feature observed earlier in spherical nuclei. It is pointed out that in deformed nuclei the coherence length corresponding to the pairing tensor has a pattern similar to what we have found previously in spherical nuclei; that is, it is maximal in the interior of the nucleus and then it decreases rather rapidly in the surface region, where it reaches a minimal value of about 2 fm. This minimal value of the coherence length in the surface is essentially determined by the finite size properties of single-particle states in the vicinity of the chemical potential and has little to do with enhanced pairing correlations in the nuclear surface. It is shown that in nuclei the coherence length is not a good indicator of the intensity of pairing correlations. This feature is contrasted with the situation in infinite matter.

DOI: 10.1103/PhysRevC.81.034307 PACS number(s): 21.30.Fe, 21.10.Re, 21.60.Jz, 24.30.Cz

I. INTRODUCTION

According to pairing models, in open-shell nuclei nucleons with energies close to the Fermi level form correlated Cooper pairs. One of the most obvious manifestations of correlated pairs in nuclei is the large cross section for two-particle transfer. In the HFB approach, commonly employed to treat pairing in nuclei, the pair transfer amplitude is approximated by the pairing tensor. In coordinate space the pairing tensor for like nucleons is defined by.

$$\kappa(\vec{r}_1 s_1, \vec{r}_2 s_2) = \langle HFB|\Psi(\vec{r}_1 s_1)\Psi(\vec{r}_2 s_2)|HFB\rangle, \tag{1}$$

where $|HFB\rangle$ is the HFB ground-state wave function, while $\Psi(\vec{r}s)$ is the nucleon field operator. By definition, the pairing tensor $\kappa(\vec{r}_1 s_1, \vec{r}_2 s_2)$ is the probability amplitude to find, in the ground state of the system, two correlated nucleons with positions $\vec{r}_1$ and $\vec{r}_2$ and with spins s_1 and s_2. This is the nontrivial part of the two-body correlations, which is not contained in the Hartree-Fock approximation.

Despite the many HFB calculations done in the last half-century, only a few studies have been dedicated to nonlocal spatial properties of the pairing tensor in atomic nuclei [1–4]. One of the most interesting properties of the pairing tensor revealed recently is its small extension in the relative coordinate $\vec{r} = \vec{r}_1 - \vec{r}_2$. Thus in Ref. [3] it was shown that the averaged relative distance, commonly called the coherence length (CL), has an unexpectedly small value in the surface of spherical nuclei, about 2–3 fm. This value is about two times lower than the shortest CL in infinite matter. Similar small values of CL were obtained later for some spherical nuclei [4] and for a slab of nonuniform neutron matter [5].

The scope of this paper is to extend the study done in Ref. [3] and to investigate axially deformed nuclei. It will be shown that in axially deformed nuclei the pairing tensor has spatial features similar to those in spherical nuclei, including a short CL in the nuclear surface. The paper is organized as follows. In Sec. II, a general expression of the pairing tensor is derived in an axially deformed harmonic oscillator (HO) basis. Expressions of the pairing tensor coupled to a total spin $S = 0$ or 1 and associated projection are also presented in three particular geometrical configurations. In Sec. III, the local as well as the nonlocal part of the pairing tensor is discussed for a few axially deformed nuclei, namely, ^{152}Sm, ^{102}Sr, and ^{238}U. Results concerning CL are also presented and interpreted in a less exclusive way compared to Ref. [3]. Summary and conclusions are given in Sec. IV.

II. PAIRING TENSOR FOR AXIALLY DEFORMED NUCLEI

As in Ref. [3], we calculate the pairing tensor in the HFB approach using the D1S Gogny force [6]. To describe axially deformed nuclei we take a single-particle basis formed by axially deformed HO wave functions. In this basis the nucleon field operators can be written as

$$\Psi(\vec{r}, s) = \sum_{m\nu} c^{+}_{ms\nu}\phi_{m\nu}(\vec{r}), \tag{2}$$

where the HO wave function is

$$\phi_{m\nu}(\vec{r}) = e^{im\theta}\Re_{|m|\nu}(\widetilde{r}) \tag{3}$$

*nathalie.pillet@cea.fr

The quantum numbers m and s are the projection of the orbital and spin momenta on the symmetry (z) axis; ν are the radial quantum numbers $\nu = (n_\perp, n_z)$. The function $\Re_{|m|\nu}(\vec{r}) \equiv \Re_{|m|\nu}(r_\perp, z)$ is given by

$$\Re_{|m|\nu}(r_\perp, z) = \varphi_{n_z}(z, \alpha_z) \times \varphi_{n_\perp m}(r_\perp, \alpha_\perp), \tag{4}$$

where

$$\varphi_{n_z}(z, \alpha_z) = \left(\frac{\alpha_z}{\pi}\right)^{\frac{1}{4}} \left[\frac{1}{2^{n_z} n_Z!}\right]^{1/2} e^{\frac{1}{2}\alpha_z z^2} H_{n_z}(z\sqrt{\alpha_z}) \tag{5}$$

and

$$\varphi_{n_\perp|m|}(r_\perp, \alpha_\perp) = \left(\frac{\alpha_\perp}{\pi}\right)^{1/2} \left[\frac{n_\perp!}{(n_\perp + |m|)!}\right]^{1/2} \times e^{\frac{1}{2}\alpha_\perp r_\perp^2} (r_\perp\sqrt{\alpha_\perp})^{|m|} L_{n_\perp}^{|m|}(\alpha_\perp r_\perp^2). \tag{6}$$

In these equations, α_z and $\alpha_\perp$ are the HO parameters in the z and perpendicular directions, which are related to the HO frequencies by $\alpha_z = M\omega_z/\hbar$ and $\alpha_\perp = M\omega_\perp/\hbar$, respectively, where M is the nucleon mass, and H_{n_z} and $L_{n_\perp}$ are the Hermite and Laguerre polynomials, respectively.

Using expansion (2) it can be shown that the pairing tensor in coordinate representation can be written in the following form (the spin up is denoted by $+$, and the spin down by $-$):

$$\begin{aligned}\kappa(\vec{r}_1+, \vec{r}_2-) &= \sum_{m_1 \geqslant 0 \nu_1 \nu_2} \Re_{|m_1|\nu_1}(\widetilde{r}_1)\Re_{|m_1|\nu_2}(\widetilde{r}_2)\Big[e^{im_1(\theta_1-\theta_2)}\, \widetilde{\kappa}^{m_1+1/2}_{m_1\nu_1,m_1\nu_2} \\ &\quad + (1-\delta_{m_1,0}) e^{-im_1(\theta_1-\theta_2)}\, \widetilde{\kappa}^{m_1-1/2}_{m_1\nu_1,m_1\nu_2}\Big], \end{aligned} \tag{7}$$

$$\begin{aligned}\kappa(\vec{r}_1+, \vec{r}_2+) &= -\sum_{m_1 \geqslant 0 \nu_1 \nu_2} [e^{im_1\theta_1 - i(m_1+1)\theta_2}\Re_{|m_1|\nu_1}(\widetilde{r}_1)\Re_{|m_1+1|\nu_2}(\widetilde{r}_2) \\ &\quad - e^{-i(m_1+1)\theta_1 + im_1\theta_2}\Re_{|m_1|\nu_1}(\widetilde{r}_2)\Re_{|m_1+1|\nu_2}(\widetilde{r}_1)] \\ &\quad \times \widetilde{\kappa}^{m_1+1/2}_{m_1\nu_1,m_1+1\nu_2}. \end{aligned} \tag{8}$$

In these expressions we have introduced the pairing tensor in the HO basis,

$$\widetilde{\kappa}_{\alpha_1\alpha_2} \equiv \widetilde{\kappa}^{\Omega}_{m_1\nu_1,m_2\nu_2} = 2s_2\langle\widetilde{0}|c_{m_1s_1\nu_1}c_{-m_2-s_2\nu_2}|\widetilde{0}\rangle = \widetilde{\kappa}_{\alpha_2\alpha_1}, \tag{9}$$

where $\Omega = m_1 + s_1 = m_2 + s_2$.

In the present study we calculate the pairing tensor corresponding to three geometrical configurations, shown in Figs. 1–3; they have the advantage of a simple separation between the center of mass (c.o.m.) $\vec{R} = (\vec{r}_1 + \vec{r}_2)/2$ and the relative $\vec{r} = \vec{r}_1 - \vec{r}_2$ coordinates.

For a finite-range force, such as the D1S Gogny force used here, the pairing tensor has nonzero values for the total spin

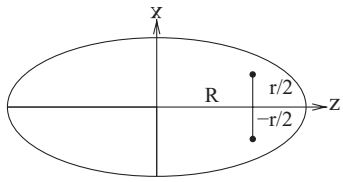

FIG. 1. Geometrical configuration (a), corresponding to two neutrons in the xz plane. R and r indicate the c.o.m. position and the relative distance of the two neutrons.

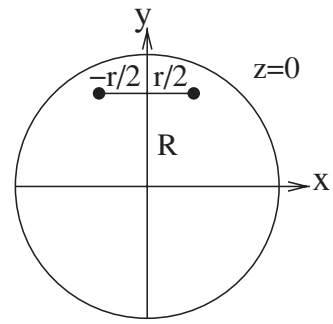

FIG. 2. Geometrical configuration (b), corresponding to two neutrons in the xy plane. R and r indicate the c.o.m. position and the relative distance of the two neutrons.

$S = 0$ and $S = 1$. How these two channels are related to the pairing tensors, Eqs. (7) and (8), depends on the geometrical configuration. Thus it can be shown that for the configuration displayed in Fig. 1, the following relations are satisfied:

$$[\kappa(\vec{r}_1s_1, \vec{r}_2s_2)]_{00} = \sqrt{2}\kappa(\vec{r}_1+, \vec{r}_2-), \tag{10}$$

$$[\kappa(\vec{r}_1s_1, \vec{r}_2s_2)]_{10} = 0, \tag{11}$$

$$[\kappa(\vec{r}_1s_1, \vec{r}_2s_2)]_{11} = [\kappa(\vec{r}_1s_1, \vec{r}_2s_2)]_{1-1} = \kappa(\vec{r}_1+, \vec{r}_2+), \tag{12}$$

where the notation $[..]_{ij}$ means that the pairing tensor is coupled to total spin $S = i$ with projection $S_z = j$.

For the configuration shown in Fig. 2 the pairing tensor $\kappa(\vec{r}_1s_1, \vec{r}_2s_2)$ is a complex quantity and we have the relations

$$[\kappa(\vec{r}_1s_1, \vec{r}_2s_2)]_{00} = \sqrt{2}\mathrm{Re}[\kappa(\vec{r}_1+, \vec{r}_2-)], \tag{13}$$

$$[\kappa(\vec{r}_1s_1, \vec{r}_2s_2)]_{10} = i\sqrt{2}\mathrm{Im}[\kappa(\vec{r}_1+, \vec{r}_2-)], \tag{14}$$

$$[\kappa(\vec{r}_1s_1, \vec{r}_2s_2)]_{11} = [\kappa(\vec{r}_1s_1, \vec{r}_2s_2)]_{1-1} = \kappa(\vec{r}_1+, \vec{r}_2+). \tag{15}$$

Finally, for configuration (c), shown in Fig. 3, we have

$$[\kappa(\vec{r}_1s_1, \vec{r}_2s_2)]_{00} = \sqrt{2}\mathrm{Re}[\kappa(\vec{r}_1+, \vec{r}_2-)], \tag{16}$$

$$[\kappa(\vec{r}_1s_1, \vec{r}_2s_2)]_{10} = 0, \tag{17}$$

$$[\kappa(\vec{r}_1s_1, \vec{r}_2s_2)]_{11} = \kappa(\vec{r}_1+, \vec{r}_2+), \tag{18}$$

$$[\kappa(\vec{r}_1s_1, \vec{r}_2s_2)]_{1-1} = \kappa(\vec{r}_1-, \vec{r}_2-) = \kappa^*(\vec{r}_1+, \vec{r}_2+). \tag{19}$$

The results for the pairing tensor shown in this paper are obtained by solving the HFB equations in a HO basis with 13 major shells for deformed nuclei. We have checked that increasing the dimension of the basis does not significantly change the spatial properties of the pairing tensor up to

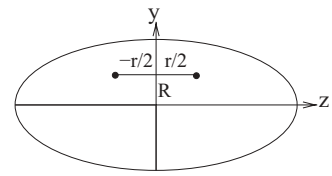

FIG. 3. Geometrical configuration (c), corresponding to two neutrons in the yz plane. R and r indicate the c.o.m. position and the relative distance of the two neutrons.

distances of about 10 fm in the nuclei studied here. This shows that a finite discrete 13-major-shell HO basis correctly describes these nuclei in the domain of interest of this work and, in particular, that continuum coupling effects can be ignored.

III. RESULTS AND DISCUSSION

A. Local and nonlocal parts of the pairing tensor

We start by briefly discussing the local part of the neutron pairing tensor. To illustrate the effect of the deformation, Fig. 4 is shows the neutron local part of the pairing tensor for ^{152}Sm calculated in the spherical configuration $\beta = 0$ and in the deformed ground state $\beta = 0.312$, where β is the usual dimensionless deformation parameter. The color scaling at the right of the plots indicates the intensity of the local part of the pairing tensor. In the spherical state the spatial structure of the local part of the pairing tensor can be simply traced back to the spatial localization of a few orbitals with energies close to the chemical potential [7]. For ^{152}Sm the most important orbitals are $2f_{7/2}$, $1h_{9/2}$, $3p_{3/2}$, and $2f_{5/2}$. As shown in Fig. 4, in the deformed state the spatial pattern of the pairing tensor is more complicated. This stems from the fact that it requires many single-particle configurations to explain its detailed structure. The spatial distribution of the configurations contributing the most to the pairing tensor are shown in Fig. 5; plots correspond to the contribution of single-particle states of given Ω and parity, with a different scaling for each plot.

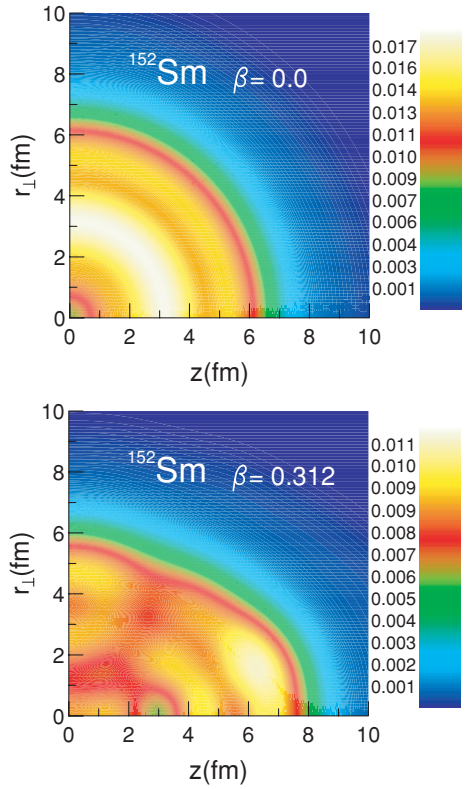

FIG. 4. (Color online) The local part of the pairing tensor for ^{152}Sm. Upper and lower panels correspond to the spherical configuration and the deformed ground state, respectively.

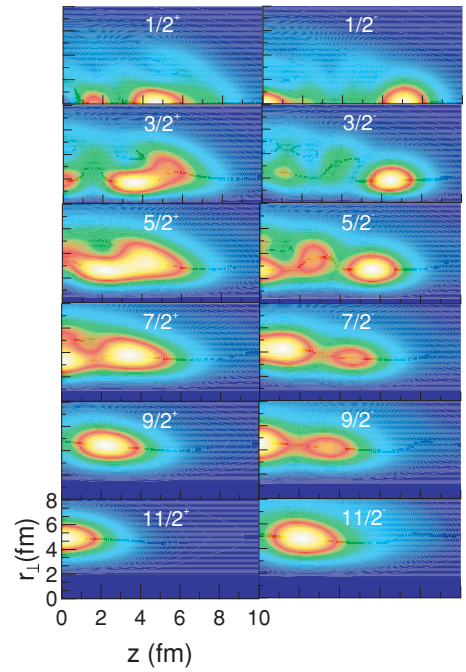

FIG. 5. (Color online) Spatial structure of the single-particle blocks Ω^π that make the largest contribution to the pairing tensor shown in the bottom panel of Fig. 4.

We focus now on the spatial structure of the nonlocal neutron pairing tensor. Figures 6–8 show some typical results for $|\kappa(\vec{R}, \vec{r})|^2$ in the three geometrical configurations (a), (b), and (c) described in Figs. 1–3 for ^{152}Sm, ^{102}Sr, and ^{238}U. At the spherical deformation, the three geometrical configurations are equivalent. For ^{102}Sr, which manifests a coexistence feature, $|\kappa(\vec{R}, \vec{r})|^2$ is shown only for the prolate minimum. For ^{238}U, the ground state as well as the isomeric state is displayed. The color scaling at the right of the plots indicates the intensity of the pairing tensor squared multiplied by a factor of 10^4. First we notice that the pairing tensor for $S = 1$ (Fig. 6, bottom) is much weaker than that for $S = 0$ (Fig. 7), by a factor of $\sim$20. This is a general feature in open-shell nuclei (the pairing channel $S = 1$ is significant in halo nuclei such as ^{11}Li). Therefore, in what follows we discuss only the channel $S = 0$.

Figures 6–8 show that with deformation the pairing tensor is essentially confined along the direction of the c.o.m. coordinate. As in spherical nuclei, the pairing tensor can be preferentially concentrated either in the surface or in the bulk, depending on the underlying shell structure. The most interesting fact shown in Figs. 6–8 is the small spreading of the pairing tensor in the relative coordinate. This is a feature we have already observed in spherical nuclei. In Ref. [3], it is reported that the predilection for small spreading in the relative coordinate is caused by parity mixing. We go back to this point in Sec. III B.

Quantitatively the spreading of the pairing tensor in the relative coordinate can be measured by the local CL defined in Ref. [8]. In the present study of deformed nuclei, as particular angular dependences are assumed according to the three geometrical configurations (a), (b), and (c), the following

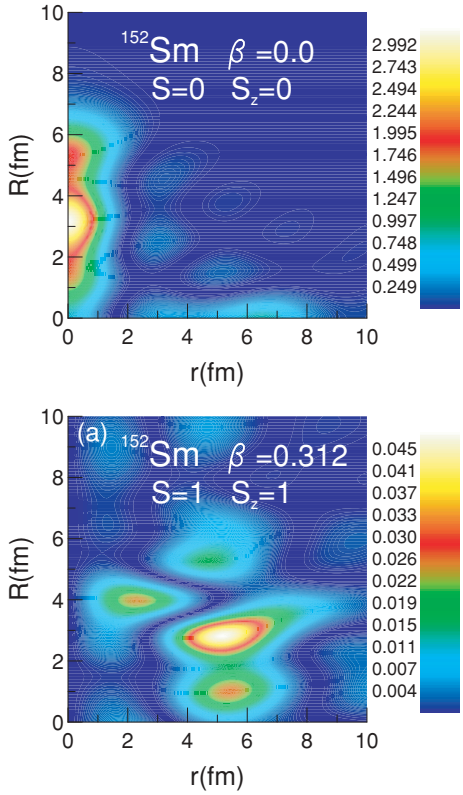

FIG. 6. (Color online) Nonlocal $\kappa(\vec{R},\vec{r})^2$ for the isotope ^{152}Sm. The deformation is indicated by β, and S is the spin. For the spherical case (upper panel), $\kappa(\vec{R},\vec{r})$ is averaged over the angles of $\vec{R}$ and $\vec{r}$. For the deformed case (lower panel), geometrical configuration (a), shown in Fig. 1, was adopted.

formula has been used:

$$\xi(R) = \sqrt{\frac{\int r^4 |\kappa(R,r)|^2 dr}{\int r^2 |\kappa(R,r)|^2 dr}}. \tag{20}$$

The pairing tensor $\kappa(R,r)$ corresponds to a given total spin $S = 0$ and a given geometrical configuration. For spherical nuclear configurations, the expression adopted for the CL is the standard one defined in Ref. [3], where averages are taken over both the angles of $\vec{R}$ and $\vec{r}$.

In Fig. 9, we present the neutron CL calculated for various deformed nuclei and configurations (a), (b), and (c) described in Figs. 1–3. We note that inside the nucleus the CL has large values, up to about 10–14 fm. This order of magnitude was already found in spherical nuclei. However, the CL displays much stronger oscillations compared to spherical nuclei, especially for geometrical configurations (a) and (b). This behavior can be attributed to the large number of different orbitals implied in pairing properties for deformed nuclei. An interesting feature shown in Fig. 9 is the pronounced minimum of about 2 fm far out in the surface that appears for all isotopes and all geometrical configurations. The minimum found here has a magnitude similar to that in spherical nuclei. We also found a small CL, ∼2 fm, in the surface of nuclei for protons. In the proton case, the Coulomb force was not taken into account in the pairing interaction but it is not expected to change the CL strongly.

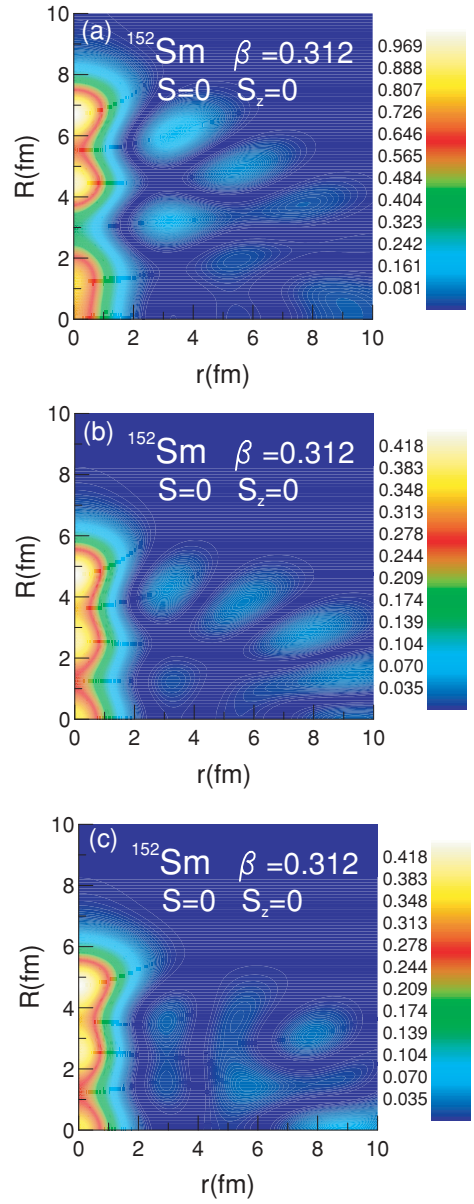

FIG. 7. (Color online) Nonlocal $\kappa(\vec{R},\vec{r})^2$ for the isotope ^{152}Sm. The deformation is indicated by β, and S is the spin. (a), (b), and (c) indicate the geometrical configurations shown in Figs. 1–3.

B. Discussion of coherence length

Compared to the smallest values of CL in nuclear matter, about 4–5 fm (see Fig. 10 for symmetric and neutronic matter), the minimal values (∼2 fm) of the CL in nuclei are astonishingly small. The question then arises, What causes such small values of CL in the surface of nuclei? Because, as just mentioned, the general behavior of the CL is similar in spherical and deformed nuclei, the following discussion focuses on spherical nuclei. As a benchmark case, we consider the isotope ^{120}Sn. In this case, the CL will be calculated as in Ref. [3],

$$\xi(\vec{R}) = \sqrt{\frac{\int r^2 |\kappa(\vec{R},\vec{r})|^2 d^3r}{\int |\kappa(\vec{R},\vec{r})|^2 d^3r}}, \tag{21}$$

where averages are taken over both the angles of $\vec{R}$ and $\vec{r}$.

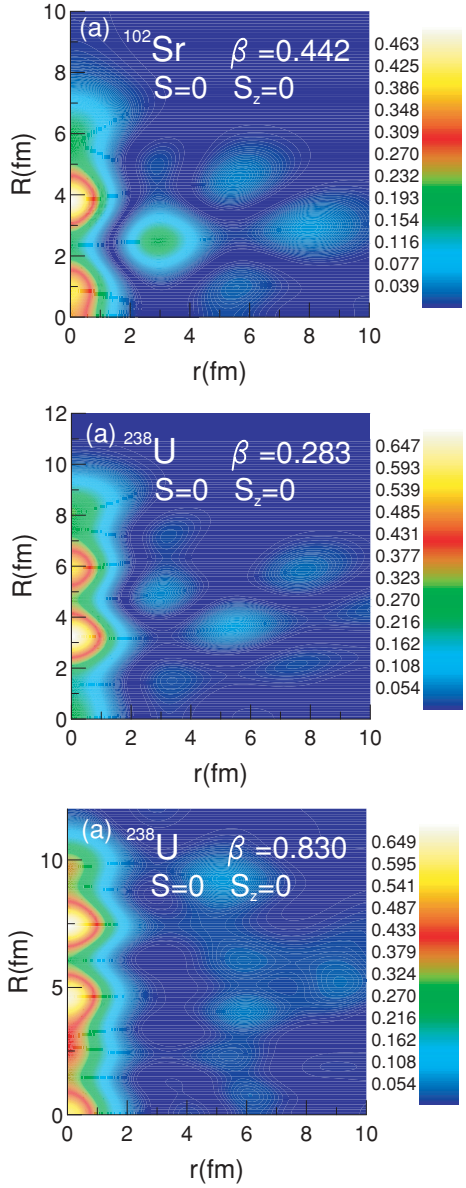

FIG. 8. (Color online) Nonlocal $\kappa(\vec{R},\vec{r})^2$ for isotopes ^{102}Sr and ^{238}U. For the latter, two cases are shown, corresponding to the ground state (middle panel) and to the fission isomer (bottom panel). Calculations were made assuming configuration (a), shown in Fig. 1.

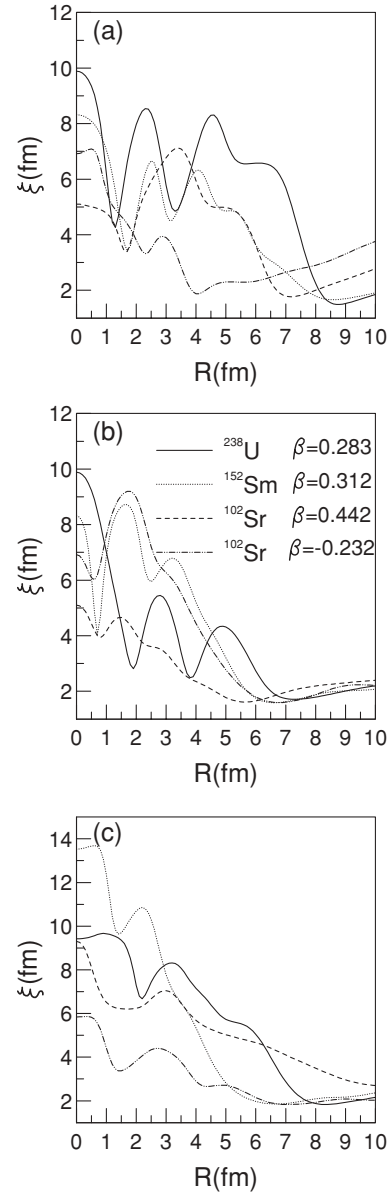

FIG. 9. Coherence length for various isotopes. β denotes the deformation, while (a), (b), and (c) are the geometrical configurations shown in Figs. 1–3.

A possible explanation for the small CL in the surface of finite nuclei could be, for example, as suggested in Ref. [3], that pairing correlations are particularly strong there. Indeed, in the surface the neutron Cooper pairs have approximatively the same size as the deuteron, a bound pair. This is a situation similar to the strong coupling regime of pairing correlations. However, it is generally believed that nuclei are in the weak coupling limit with respect to pairing [9]. In what follows, we examine whether there exists a correspondence between the magnitude of the CL and an enhancement of pairing correlations in the nuclear surface. Even though a local view can only give an incomplete picture because of fluctuations, a quantity that can be used to explore the spatial distribution of pairing correlations is the local pairing energy,

$$E_c(R) = -\int d^3r\, \Delta(\vec{R},\vec{r})\kappa(\vec{R},\vec{r}), \tag{22}$$

where $\Delta(\vec{R},\vec{r})$ is the nonlocal pairing field. In practice, in Eq. (22), we use the angle-averaged quantities.

The localization properties of $E_c(R)$ are shown in Fig. 11 (black line), which displays the results for several spherical nuclei. We note that in the surface region, where the minimum CL is located, there is a local maximum of $|E_c(R)|$ present for all nuclei considered. The largest (absolute) value of $E_c(R)$ is not necessarily located in the surface region and the oscillations of the inner part of the distributions seem to be caused mostly by shell fluctuations.

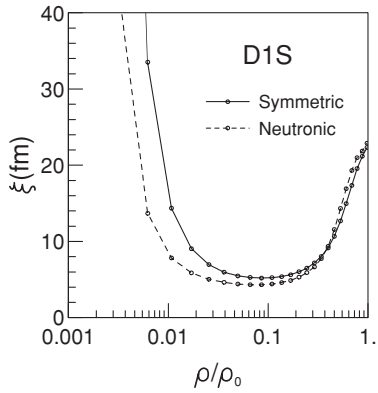

FIG. 10. Coherence length in symmetric and neutronic matter according to the density normalized to the saturation density and calculated with the D1S Gogny force.

To better exhibit a surface enhancement of pairing correlations, we have to consider a normalized pairing energy, otherwise the strong fall-off of the density will mask the local increase in pairing to a great extent. One could divide $E_c(R)$ by the local density, as done in Eq. [1]. However, here we prefer to divide by the local pairing density $\kappa(R) = \kappa(R, 0)$, leading to the following definition of an average local pairing field

$$\Delta_{av}(R) = \frac{1}{\kappa(R)} \int d^3r \, \Delta(\vec{R}, \vec{r}) \kappa(\vec{R}, \vec{r}). \tag{23}$$

In practice, in Eq. (23) we again use the angle-averaged quantities. We remark that with a zero-range pairing force, the preceding definition of the average pairing field gives the local pairing field. The localization properties of $\Delta_{\rm av}(R)$ are shown in Fig. 11 (bottom line). We notice a qualitatively similar behavior as for $E_c(R)$. However, owing to the normalization, the average pairing field has significant values out in the surface region. Closer inspection of Fig. 11 shows that the averaged pairing field reaches 20% farther out into the surface of the nucleus compared to the particle density (blue line). This can be quantified by the corresponding root mean square values. This push of pairing correlations to the external region is determined by the localization properties of orbitals from the valence shell, which give the main contribution to the pairing tensor and pairing field. Because these states are less bound they are more spatially extended than the majority of states that determine the particle density and the nuclear radius. Moreover, the increase in the effective mass in the surface also probably plays an important role. Like the local pairing energy $E_c(R)$, the average pairing field $\Delta_{\rm av}(R)$ presents a generic local maximum in the surface region with a local enhancement of pairing correlations (at tenth the matter density in ^{120}Sn, the average pairing field still reaches the relatively large value of $\sim$0.5 MeV). On the contrary, this maximum is not necessarily an absolute one and higher pairing field values can appear in the interior of nuclei, depending on the underlying shell structure.

To understand whether this local enhancement of pairing correlations can explain the minimum value of $\sim$2 fm of the CL in the surface of finite nuclei, we have calculated the CL under the same conditions as before but with a variable factor

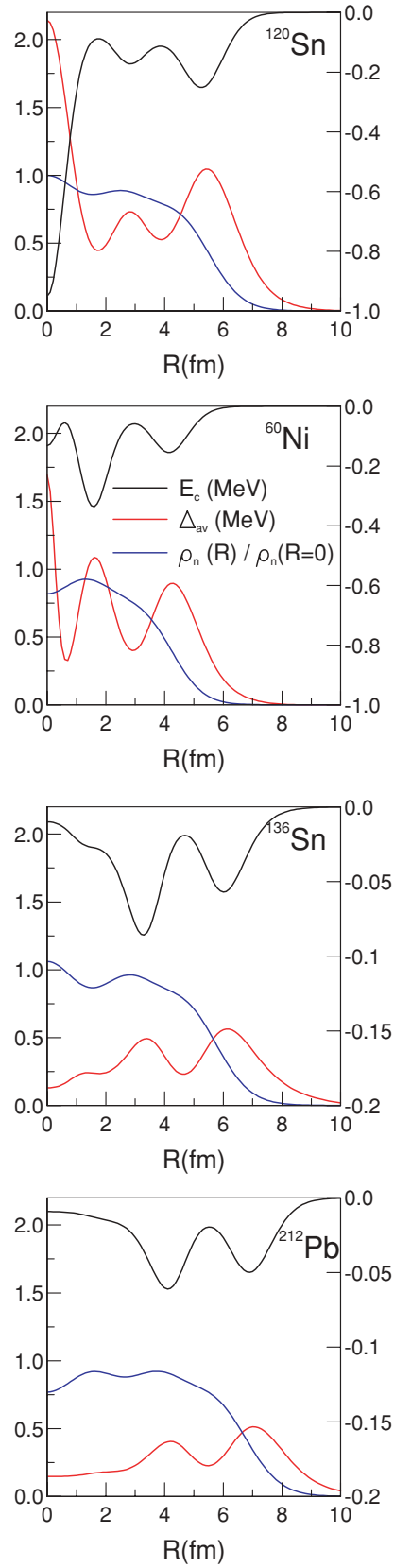

FIG. 11. (Color online) Pairing correlation energies (right scale; MeV) and average pairing fields (left scale; MeV in ^{120}Sn, ^{60}Ni, ^{136}Sn, and ^{212}Pb. The blue line shows the neutron density relative to its value in the center of the nucleus (left scale).

α in front of the ($S = 0$, $T = 1$) pairing intensity of the D1S Gogny force (and only there). The result is shown in Fig. 12 for ^{120}Sn with α between 1.0 and 0.5 (top). It should be mentioned that for $\alpha = 1.0$, the ^{120}Sn pairing energy is equal to $\sim$19 MeV, whereas for $\alpha = 0.5$ it is $\sim$0.5 MeV, which can be considered as a very weak pairing regime. Despite these extreme variations of the pairing field, the values of CL change very little overall, except for $R \leqslant 1$ fm. At $R \simeq 6$ fm, the variation is less than 0.2 fm. As we will see, this behavior is completely different in nuclear matter. From this study, it becomes clear that the CL is practically independent of the pairing intensity, in particular, in the surface of finite nuclei.

Therefore, we must revisit the interpretation proposed in our preceding paper [3], that the minimal size of $\sim$2 fm of Cooper pairs in the nuclear surface is a consequence of particularly strong local pairing correlations. From the fact that completely different behavior is obtained in infinite nuclear matter (see the following and Fig. 16), the small size of the CL in the surface of nuclei seems to be strongly related to the finite size of the nucleus.

At this stage of our analysis, it is important to clarify the role of parity mixing that was put forward in our preceding work [3] on the behavior of the CL. The bottom panel in Fig. 12 displays the CL calculated either with the even part of the pairing tensor κ_e or with the odd one κ_o, for the same values of α as before. In both cases, the value of the CL does not depend much on the intensity of the pairing. This conclusion holds here

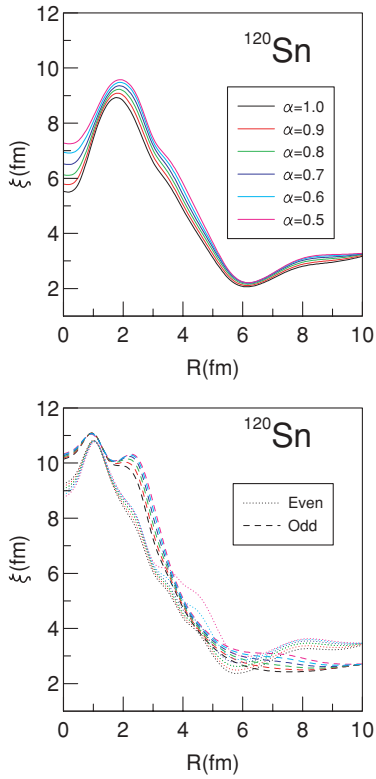

FIG. 12. (Color online) Coherence length calculated with the total pairing tensor κ (top panel) and the even κ_e and odd κ_o parts of the total pairing tensor (bottom panel) for different intensities of pairing strength, in the case of ^{120}Sn.

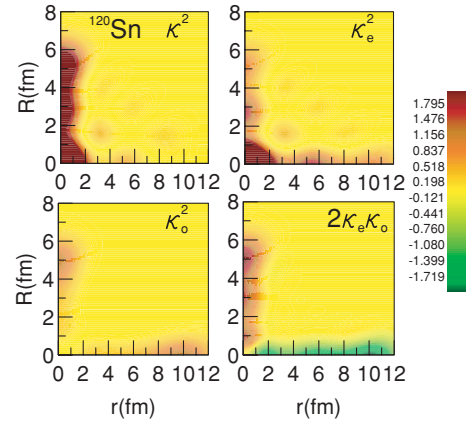

FIG. 13. (Color online) Nonlocal part of the pairing tensor κ^2 and even κ_e^2 and odd κ_o^2 parts of the nonlocal part of the pairing tensor and the interference term $2\kappa_e\kappa_o$ for ^{120}Sn.

for all values of R. Comparing the curves in the two panels in Fig. 12, one sees that the even/odd CLs have reasonably larger values in the center of the nucleus ($\sim$10 fm) than those calculated with the full κ (6–8 fm), almost independently of the value of α. In the surface region they are practically of the same magnitude (2–3 fm). These results indicate that the parity mixing discussed in Ref. [3] influences the CL essentially for small values of R. Therefore, parity mixing cannot be the main reason for the small value of the CL in the surface region.

The trends shown in Fig. 12 can be traced back to the variations of κ^2 as well as κ_e^2, κ_o^2, and the interference term $2\kappa_e\kappa_o$ plotted in Fig. 13. The interference term is large only along the axes $r = 0$ and $R = 0$. However, in calculating the CL, $|\kappa|^2$ is multiplied by a factor r^4 in the numerator of Eq. (21). Hence, the large values of this interference term near the $r = 0$ axis will not come into play significantly. Therefore, as observed previously, parity mixing will be significant essentially for $R \lesssim 1$ fm.

This observation is confirmed by looking at the quantity

$$X(R, r) = \frac{r^4 |\kappa(R, r)|^2}{N(R)}, \tag{24}$$

where $N(R) = \int_0^\infty dr r^2 \kappa(R, r)^2$. This quantity, once integrated over r, yields the square of the CL, Eq. (21) namely, $\xi^2(R) = \int_0^\infty X(R, r) dr$.

$X(R, r)$ is presented in Fig. 14 for four values of R, namely, 0, 3, 6, and 9 fm, corresponding to the interior of the nucleus and the vicinity of the surface. The results are displayed for various values of the pairing factor α.

Except for $R = 0$, $X(R, r)$ and hence $\xi(R)$ are not really sensitive to the strength of the pairing interaction. The large dependence of $X(R, r)$ on the pairing strength at $R = 0$ comes from the comparatively large parity mixing already mentioned in connection with Fig. 13, which is negative and maximum in absolute value for $r \simeq 10$ fm. Because the parity mixing tends to disappear as the pairing strength decreases, the height of the peak at $r = 10$ fm increases. In contrast, for $R = 3$, 6, and 9 fm the influence of parity mixing is very modest and the behavior of $X(R, r)$ is determined essentially by κ_e^2 and κ_o^2. From $R \simeq 3$ fm to $R \simeq 6$ fm, one observes a sensitive

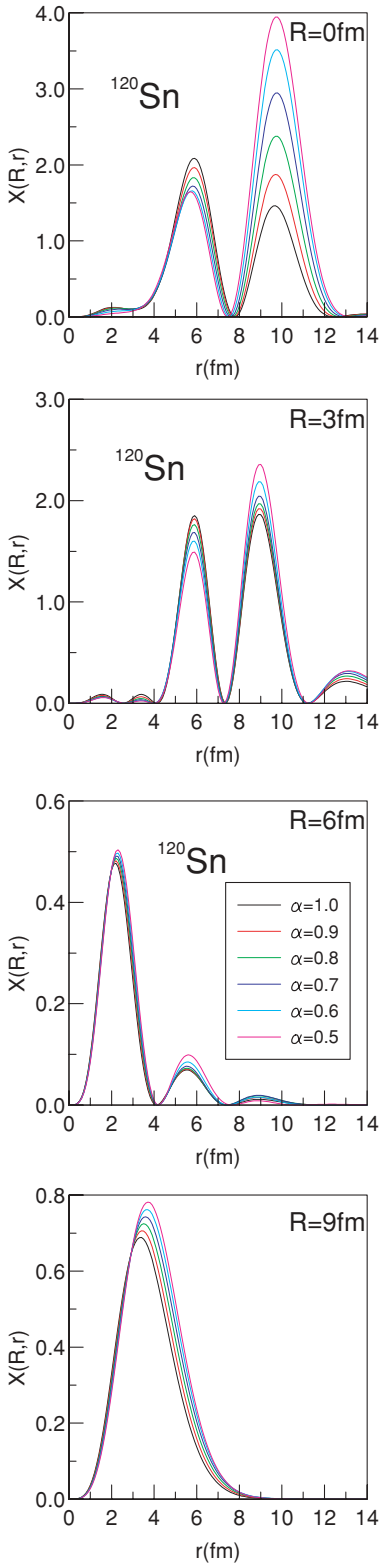

FIG. 14. (Color online) $X(R, r)$ for $R = 0$, 3, 6, and 9 fm in the case of ^{120}Sn.

reduction of the magnitude of $X(R, r)$, leading to a lowering of the CL. In the vicinity of the surface ($R \geqslant 6$ fm), the oscillatory behavior of $X(R, r)$ disappears. Here, single-particle wave functions have almost reached their exponential regime. This

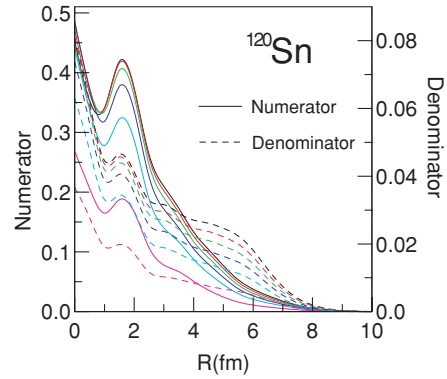

FIG. 15. Evolution of the numerator and denominator of $\xi(R)$ for various values of α, in the case of ^{120}Sn.

explains why, at $R \geqslant 6$ fm, $X(R, r)$ is characterized by only one major peak. The width of this major peak is minimum at the nuclear surface. Its broadening for $R = 9$ fm explains the increase in the CL beyond the nuclear surface.

A more global way to analyze the behavior of the CL is to consider directly the dependence on R of the numerator and the denominator of Eq. (21). This is shown in Fig. 15.

One sees that, independently of the value of α (the color code is the same as for Fig. 12), the denominator decreases faster than the numerator around $R = 6$ fm and beyond. This sudden change in the slope of the denominator is accountable for the minimum value of CL.

A similar analysis of the CL and of the influence of pairing correlations was carried out in infinite matter. In Fig. 16, we show the CL in infinite symmetric nuclear matter as a function of the density ρ normalized to its saturation value ρ_0, for the same α values as in the HFB calculations for finite nuclei. In the nuclear matter case, we see that the CL depends very strongly on the pairing intensity, whatever the density. For instance, the minimum value of CL increases a lot as pairing decreases. This behavior can be understood from an approximate analytic evaluation of the CL in infinite nuclear matter based on the definition, Eq. (21), which differs only slightly from the usual

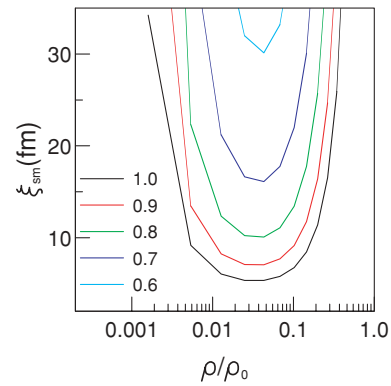

FIG. 16. (Color online) Coherence length calculated with different intensities of pairing strength in symmetric nuclear matter.

Pippard expression [10] (see Appendix):

$$\xi_{\rm nm} = \frac{\hbar^2 k_F}{2\sqrt{2}m^*|\Delta_F|}\left[1 + \frac{a^2}{8}(3b^2 - 12b + 4) + \mathcal{O}(a^3)\right], \tag{25}$$

where $a = |\Delta_F|/|\epsilon_F|$, $b = k_F\Delta'_F/\Delta_F$, with Δ_F and Δ'_F the pairing field and its derivative for the Fermi momentum k_F. As discussed in Appendix, the correction terms in Eq. (25) are very small.

We see that the CL in infinite matter varies approximatively inversely proportional to the gap at the Fermi surface. This behavior is at variance with the results in finite nuclei, particularly where the CL shows the minimum; see Fig. 12. This clearly indicates that the behavior of the CL, in particular, the small value obtained in the surface of finite nuclei, is strongly influenced by the structure of the orbitals and that pairing plays a secondary role.

To examine this question in more detail, we show in Fig. 17 the extension of completely uncorrelated pairs made of Hartree-Fock neutron single-particle wave functions. We use a definition of the extension of the pair size similar to the CL of Eq. (21) namely,

$$\xi_{\rm orb}({\rm R}) = \frac{(\int r^2|A_i(\vec{R},\vec{r})|^2 d^3r)^{1/2}}{(\int |A_i(\vec{R},\vec{r})|^2 d^3r)^{1/2}}. \tag{26}$$

The uncorrelated-pair wave function $A_i(\vec{R},\vec{r})$ is defined as

$$\begin{aligned} A_i(\vec{R},\vec{r}) = {} & \frac{1}{4\pi}(2j_i+1)\sum_{n_\alpha n_\beta} C^{n_i l_i j_i}_{n_\alpha} C^{n_i l_i j_i}_{n_\beta} \\ & \times \sum_{nNl}(-)^l \frac{(2l+1)^{1/2}}{2l_i} u_{nl}(r/\sqrt{2}) u_{Nl}(\sqrt{2}R) \\ & \times P_l(\cos\theta)\langle nlNl;0|n_\alpha l_i n_\beta l_i 0\rangle, \end{aligned} \tag{27}$$

where $C^{n_i l_i j_i}_{n_\alpha}$ is the component of the $(n_i l_i j_i)$ neutron single-particle orbital on the HO basis function $(n_\alpha l_i j_i)$. This equation is the same as Eq. (3) in Ref. [3], with the matrix $\kappa^{l_i j_i}_{n_\alpha n_\beta}$ of the pairing tensor replaced with the product of the two C coefficients.

Because $\xi_{\rm orb}(R)$ corresponds to two noninteracting neutrons put into the same orbit and coupled to $(L = 0,\ S = 0)$, it contains only the correlations induced by the confinement of the single-particle wave functions. As Fig. 17 shows, $\xi_{\rm orb}$ has a pattern rather similar to the global CL displayed in Figs. 9 and 12, except for the $3s_{1/2}$ orbital. Thus, provided that this orbital is not strongly populated, a change in the relative contributions of the single-particle states in the pairing tensor, for example, induced by varying the intensity of pairing correlations, will not cause significant modifications of the global CL. This result was also found by Pastore [11].

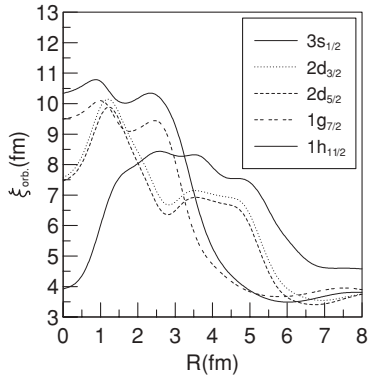

FIG. 17. Coherence length for Hartree-Fock single-particle orbitals of the neutron valence shell of ^{120}Sn.

From Fig. 17 we see that (except for $3s_{1/2}$), $\xi_{\rm orb}(R)$ exhibits a minimum in the surface of the order of $\simeq$3.5 fm. This is indeed small but still larger than the 2.3 fm found with Eq. (21) for $\alpha = 1$ (or 2.5 fm for $\alpha = 0.5$). The reduction by about 30%, from 3.5 to 2.3 fm, of the minimum of the CL is very likely because, even for very small pairing, some orbit mixing takes place (remember that the influence of pairing is compensated in the ratio of numerator to denominator and that the chemical potential is not necessarily locked to a definite level but may stay in between levels). The cross terms of the wave functions can be negative, yielding a possible explanation of the effect. Let us also point out that the CL implying only the even part of the pairing tensor (or the odd one), see Ref. [3], is of the order of $\sim$2.7 fm for ^{120}Sn; see Fig. 12. Therefore, there should exist a slight influence of parity mixing in the CL calculated with the full κ.

Nonetheless, the preceding discussion clearly indicates that the small value of the CL in the surface of finite nuclei is essentially caused by the structure of the single-particle wave functions. Our conclusion is somewhat different from the one put forward in our early paper [3]. There, we had not explored the behavior of the CL as a function of the pairing strength, which led us to conclude that the small size of Cooper pairs stems from a local strong coupling pairing regime. However, the other results and conclusions of Ref. [3] still hold.

One may speculate about the reason for this radically different behavior of the CL in nuclei and infinite nuclear matter. One issue that certainly can be invoked is that, in macroscopic systems, the number of single-particle states in an energy range of the order of the gap is huge, whereas in nuclei there are only a few states per MeV. To examine this effect more precisely, let us consider, for convenience, the example of a spherical HO potential. We want to keep the essential finite size effects but eliminate unessential shell effects. It is well known that this can be achieved via so-called Strutinsky smoothing. Single shells are washed out and what remains is a continuum model with energy as a variable, instead of individual discrete quantum states. Therefore for the pairing tensor in Wigner space, we can write

$$\kappa(\vec{R},\vec{p}) = \int_E dE\kappa(E) f(E;\vec{R},\vec{p}), \tag{28}$$

where $\kappa(E) = u_E v_E$ is the Strutinsky averaged pairing tensor [12] and $f(E;\vec{R},\vec{p})$ is the Strutinsky averaged Wigner transform of the density matrix on the energy shell E [13]. Integration of this quantity over energy up to the Fermi level yields the Strutinsky averaged density matrix in Wigner space. The latter quantity is shown in Fig. 1 of Ref. [14].

A particularity of the Strutinsky smoothed spherical HO is that all quantities depend on $\vec{R}$ and $\vec{p}$ only via the classical

Hamiltonian $H_{\rm cl}(\vec{R},\vec{p})$. We see that the Wigner transform of the density matrix is approximately constant for energies below the Fermi energy and drops to zero within a width of order $\hbar\omega$. The corresponding density matrix on the energy shell can then be obtained from the quantity shown in Ref. [14] by differentiation with respect to energy. We, therefore, deduce that $f(E;H_{\rm cl})$ is peaked around $E\sim H_{\rm cl}$, with a width of order $\hbar\omega$.

The preceding integral over E in $\kappa(\vec{R},\vec{p})$ is, therefore, a convolution of two functions, one of width $\sim\Delta$ and the other of width $\sim\hbar\omega$. As long as the gap is smaller than $\hbar\omega$, the $\vec{R}$ and $\vec{p}$ behavior of κ will be dominated by $f(E;H_{\rm cl})$, that is, by the oscillator wave functions. This is what happens in finite nuclei. On the contrary, in infinite matter or in LDA descriptions, $f(E;\vec{R},\vec{p})$ is a δ function, $\delta(E-H_{\rm cl})$, and then the $\vec{R}$, $\vec{p}$ behavior of $\kappa(\vec{R},\vec{p})$ is entirely determined by the width of $\kappa(E)$, that is, by the intensity of pairing.

This interpretation qualitatively explains the very different behaviors of the CL with respect to the magnitude of pairing in finite nuclei and infinite matter. It also explains why the value of the CL in the surface of finite nuclei can be much smaller than that calculated in infinite nuclear matter at any density.

More quantitative investigations along this line are in preparation [15].

IV. CONCLUSIONS

In this paper we have continued our study of the spatial properties of pairing correlations in finite nuclei. We first generalized our previous work [3] to deformed nuclei and found that the spatial behavior of pairing is rather similar to that in the spherical case. This concerns, for instance, the remarkably small value of the CL ($\simeq$2 fm) in the nuclear surface. Farther inside the nucleus, more pronounced differences sometimes appear. We then concentrated on the reason for this strong minimal extension of the CL in the surface of nuclei. It was found that this feature is practically independent of the intensity of pairing and seems to survive even in the limit of very small pairing correlations. A detailed analysis of the quantities entering the definition of the CL indicates that, in finite nuclei, the latter is mainly determined by the single-particle wave functions, that is, by finite size effects. This eliminates suggestions that the strong observed lowering of the CL in the nuclear surface has something to do with especially strong pairing correlations in the surface [3] or in a surface layer, that is, with a two-dimensional effect [16]. A particular situation seems to prevail in the two-neutron halo state of ^{11}Li [17].

We have also made the same study in infinite nuclear matter. We found that in that case the CL depends strongly on the gap, and an approximate inverse proportionality between the gap and the CL could be established. Concerning the reason why nuclei and infinite matter behave so differently with respect to the CL, we put forward the fact that the number of levels in the range of the gap value is huge in a macroscopic system, whereas there are only a handful of levels in finite nuclei. In such situations the numerator and denominator in the definition of the CL have a similar dependence on pairing and its influence tends to cancel. From this work, it appears that the CL may not be a good indicator of the spatial structure of pairing correlations in the case of nuclei or of other finite systems with a weak coupling situation such as certain superconducting ultrasmall metallic grains [18]. This fact should not make us forget that, for other quantities, pairing in nuclei can have a strong effect, as is well known. For example, the pairing tensor itself, as studied in this work, is very sensitive to parity mixing (see Fig. 13), where a strong redistribution, that is, a concentration of pairing strength along the c.o.m. positions of the pairs, takes place. Such a feature probably is responsible for the strong enhancement of pair transfer into superfluid nuclei [19]. This small extension of the pairing tensor in the relative coordinate may be present not only in the surface but also in the bulk, depending somewhat on the shell structure. However, on average a generic but moderate enhancement of pairing correlations (obtained with the D1S Gogny force) is present in the nuclear surface; see Fig. 11. Further elaboration of these aspects will be given in a forthcoming paper [15].

ACKNOWLEDGMENTS

We thank A. Pastore for sending us clarifying information and for fruitful discussions. We also acknowledge K. Hagino, Y. Kanada-Enyo, M. Matsuo, A. Machiavelli, H. Sagawa, and X. Viñas for useful discussions. This work was partially supported by the Romanian Authority for Scientific Research through Grant Idei No. 270.

APPENDIX: NEUTRON COHERENCE LENGTH IN INFINITE NUCLEAR MATTER

Introducing the Wigner transform,

$$\kappa_W(\vec{R},\vec{k})=\int d^3r\,\kappa(\vec{R},\vec{r})e^{i\vec{k}\vec{r}}, \tag{A1}$$

of the HFB neutron pairing tensor $\kappa(\vec{R},\vec{r})$, the CL defined by Eq. (21) can be rewritten as

$$\xi(\vec{R})=\sqrt{\frac{\int d^3k|\vec{\nabla}_k\kappa_W(\vec{R},\vec{k})|^2}{\int d^3k|\kappa_W(\vec{R},\vec{k})|^2}}. \tag{A2}$$

In infinite nuclear matter, κ_W is independent of $\vec{R}$, depends on $\vec{k}$ only through the length $k=|\vec{k}|$, and is given by $\kappa_W(k)=\Delta(k)/2E(k)$, where $\Delta(k)$ is the HFB neutron pairing field and $E(k)=\sqrt{[e(k)-\mu]^2+\Delta(k)^2}$ the neutron quasiparticle energies, with $e(k)$ the single-neutron energies and μ the neutron chemical potential. Substituting these expressions into Eq. (A2) yields $\xi_{\rm nm}=\sqrt{N/D}$, with

$$\begin{aligned} N&=\int_0^\infty k^2dk\,\frac{[e(k)-\mu]^2\{\Delta'(k)[e(k)-\mu]-\Delta(k)e'(k)\}^2}{\{[e(k)-\mu]^2+\Delta(k)^2\}^3},\\ D&=\int_0^\infty k^2dk\,\frac{\Delta(k)^2}{[e(k)-\mu]^2+\Delta(k)^2}. \end{aligned} \tag{A3}$$

The primed quantities are first derivatives. To be able to express the integrals analytically, we introduce the following three approximations:

(i) $\mu\simeq e(k_F)\equiv e_F$, where k_F is the neutron Fermi momentum.

(ii) $e(k) \simeq \hbar^2 k^2/(2m^*)$, where m^* is the k_F-dependent neutron effective mass.

(iii) In the usual situation of nuclear physics, where the gap values are much smaller than the Fermi energy, the functions under the two integrals, Eqs. (A3), are sufficiently peaked around $k = k_F$ so that one can take $\Delta(k) \simeq \Delta(k_F) \equiv \Delta_F$ and $\Delta'(k) \simeq \Delta'(k_F) \equiv \Delta'_F$.

Using these assumptions and making the change of variables $k = xk_F$, expressions (A3) become

$$N = a^2 k_F \int_0^\infty \frac{x^2(x^2-1)^2[b(x^2-1)-2x]^2}{[(x^2-1)^2+a^2]^3} dx,$$
$$D = a^2 k_F^3 \int_0^\infty \frac{x^2}{(x^2-1)^2+a^2} dx, \tag{A4}$$

with $a = |\Delta_F/e_F|$, $b = k_f \Delta'_F/\Delta_F$. Assuming $a \neq 0$, the integrals on the right-hand sides of Eqs. (A4) can be calculated analytically using contour integration in the complex plane and the method of residues. (More precisely, the integrand for N can be broken into an even function for which the integration range, as that for D, can be extended from $-\infty$ to $+\infty$ and integrated by the method of residues, and an odd function that is easily integrated after the change of variable $y = x^2$). One gets

$$N = a^2 k_F \left\{ 2\pi \left(aY \sqrt{\frac{1+\sqrt{1+a^2}}{2}} - X \sqrt{\frac{-1+\sqrt{1+a^2}}{2}} \right) - \frac{b}{4a} \left[\frac{3\pi}{2} + 3\cot^{-1}(a) - \frac{a}{1+a^2} \right] \right\},$$
$$D = \frac{\pi}{2} a k_F^3 \sqrt{\frac{1+\sqrt{1+a^2}}{2}}, \tag{A5}$$

where X and Y are functions of a and b given by

$$X = \frac{a^2 b^2 (4a^2+5) - 2(1+a^2)(5a^2+2)}{64\, a^2 (1+a^2)^2},$$
$$Y = \frac{a^2 b^2 (21a^4+35a^2+12) + 4(1+a^2)(7a^2+4)}{128\, a^4 (1+a^2)^2}. \tag{A6}$$

Usually, a is much smaller than 1, even at low densities. Expanding Eqs. (A6) around $a = 0$, one obtains

$$\xi_{\rm nm} \sim \frac{1}{ak_F\sqrt{2}} \left[1 + \frac{a^2}{8}(3b^2 - 12b + 4) + \mathcal{O}(a^3) \right]. \tag{A7}$$

With $a = |\Delta_F|/(\hbar^2 k_F^2/2m^*)$, the leading term yields

$$\xi_{\rm nm} \sim \frac{1}{2\sqrt{2}} \frac{\hbar^2 k_F}{m^* |\Delta_F|}. \tag{A8}$$

This expression is very close to the Pippard approximation of the CL [10],

$$\xi_{\rm Pippard} = \frac{1}{\pi} \frac{\hbar^2 k_F}{m^* |\Delta_F|}, \tag{A9}$$

the prefactor being $1/2\sqrt{2} \sim 1/2.8$ instead of $1/\pi$. Usual values of a and b show that the first correction term in Eq. (A7) is very small. For instance, in symmetric nuclear matter at one-tenth the normal density, one gets $k_F \simeq 0.6\,\text{fm}^{-1}$, $a \simeq 0.2$, and $b \simeq 0.3$ with the Gogny effective force, which yields 3.10^{-3} for this term. The next terms can be shown to be even smaller. Moreover, numerical evaluations of the integrands in Eqs. (A3) for the Gogny force show that the three preceding approximations employed for deriving Eqs. (A5), in particular, the third one, are extremely well justified for densities ranging from zero to twice the normal density in symmetric nuclear matter.

[1] M. A. Tischler, A. Tonina, and G. G. Dussel, Phys. Rev. C **58**, 2591 (1998).

[2] M. Matsuo, K. Mizuyama, and Y. Serizawa, Phys. Rev. C **71**, 064326 (2005).

[3] N. Pillet, N. Sandulescu, and P. Schuck, Phys. Rev. C **76**, 024310 (2007).

[4] A. Pastore, F. Barranco, R. A. Broglia, and E. Vigezzi, Phys. Rev. C **78**, 024315 (2008).

[5] S. S. Pankratov, E. E. Saperstein, M. V. Zverev, M. Baldo, and U. Lombardo, Phys. Rev. C **79**, 024309 (2009).

[6] J. Dechargé and D. Gogny, Phys. Rev. C **21**, 1568 (1980); J.-F. Berger, M. Girod, and D. Gogny, Comput. Phys. Commun. **63**, 365 (1991).

[7] N. Sandulescu, P. Schuck, and X. Vinas, Phys. Rev. C **71**, 054303 (2005).

[8] F. V. De Blasio, M. Hjorth-Jensen, O. Elgaroy, L. Engvik, G. Lazzari, M. Baldo, and H.-J. Schulze, Phys. Rev. C **56**, 2332 (1997).

[9] A. Bohr and B. Mottelson, *Nuclear Structure*, Vol. II (Benjamin, New York, 1975), p. 398.

[10] A. L. Fetter and J. D. Walecka, *Quantum Theory of Many-Particle Systems* (McGraw-Hill, New York, 1971).

[11] A. Pastore, Ph.D. thesis, Politecnico di Milano, 2008; A. Pastore (private communication).

[12] M. Brack and P. Quentin, Nucl. Phys. A **361**, 35 (1981).

[13] X. Viñas, P. Schuck, M. Farine, and M. Centelles, Phys. Rev. C **67**, 054307 (2003).

[14] M. Prakash, S. Shlomo, and V. M. Kolomietz, Nucl. Phys. A **370**, 30 (1981).

[15] X. Viñas, P. Schuck, and N. Pillet, arXiv:1002.1459v1 [nucl-th].

[16] Y. Kanada Enyo, N. Hinohara, T. Suhara, and P. Schuck, Phys. Rev. C **79**, 054305 (2009).

[17] K. Hagino, H. Sagawa, J. Carbonell, and P. Schuck, Phys. Rev. Lett. **99**, 022506 (2007); arXiv:0912.4792v1 [nucl-th].

[18] J. von Delft and D. C. Ralph, Phys. Rep. **345**, 61 (2001).

[19] W. von Oertzen and A. Vitturi, Rep. Prog. Phys. **64**, 1247 (2001).